Supplement of Atmos. Chem. Phys., 23, 14761–14778, 2023
https://doi.org/10.5194/acp-23-14761-2023-supplement

Atmospheric Chemistry and Physics
Open Access

Supplement of

Nitrous acid budgets in the coastal atmosphere: potential daytime marine sources

Xuelian Zhong et al.

Correspondence to: Hengqing Shen (hqshen@sdu.edu.cn) and Likun Xue (xuelikun@sdu.edu.cn)

Texts

S1. Sensitivity analysis of HONO in dust and photochemical periods

According to the parameter ranges in Table S4, we conducted a sensitivity analysis on the effects of different parameter selections on HONO concentrations during dust and photochemical pollution days. The results are provided in Figure S3 and Figure S4, and a summary of the findings can be found in Table S5. Overall, heterogeneous reactions of NO_2 during dust days and photolysis of nitrate during photochemical pollution days are important sources of HONO. However, the choice of different parameters can affect the relative importance of these pathways. In general, based on the current parameter selection, the HONO concentrations can be reasonably simulated, but future research should focus on more detailed studies of the parameters for different HONO formation pathways in various environments.

S2. Calculation of enhancement factor (EF)

$$EF = \frac{P_{missing}}{JHNO_3 \times [pNO_3^-]} \quad \text{(SE1)}$$

$$P_{missing} = [HONO]\times J_{HONO} + [HONO]\times[OH]\times k_{OH+HONO} + [HONO]\times k_{deposition} - [NO]\times[OH]\times k_{OH+NO} - [NO_2]\times(k_{ground} + k_{ground,\,hv} + k_{aerosol} + k_{aerosol,\,hv}) - HONO_{emission} \quad \text{(SE2)}$$

In Equation SE1, $P_{missing}$ represents the missing HONO production rate, which is calculated using Equation SE2 with model results (10^{-9} mol m^{-3} s^{-1}). [pNO_3^-] denotes the particulate nitrate concentration (10^{-9} mol m^{-3}). To estimate the enhancement factor of J(pNO_3^-), we subtract the contributions of HONO sources except for the photolysis of pNO_3^-. The calculated EF value is approximately 4000, which is significantly higher than the EF value used in Equation 7 (around 118). The photolysis rate of pNO_3^- increases to about 2.8×10^{-3} s^{-1}, which is substantially greater than the rates reported in previous studies (no more than 10^{-3} s^{-1}) as summarized by Andersen et al. (2023).

Tables

Table S1. Summary of the "sea case" and "land case".

Number	Sea case (less than 1 h traveling time over the land)	Number	Land case (less than 1 h traveling time over the sea)
1	4/28 0:00–4:00	1	4/27 17:00–19:00, 21:00
2	4/29 1:00–6:00	2	4/28 8:00–9:00, 15:00–19:00
3	4/30 12:00–23:00	3	4/29 15:00–23:00
4	5/1 0:00–1:00	4	4/30 0:00–8:00
5	5/2 17:00–23:00	5	5/1 3:00–5:00, 8:00–16:00
6	5/3 0:00–23:00	6	5/2 9:00–11:00
7	5/4 0:00–6:00	7	5/4 9:00–17:00, 22:00–23:00
8	5/5 19:00–23:00	8	5/5 0:00–15:00
9	5/7 21:00–23:00	9	5/7 1:00–18:00
10	5/8 0:00–1:00	10	5/8 10:00–13:00
11	5/9 1:00–23:00	11	5/16 23:00
12	5/10 0:00–23:00	12	5/17 7:00–19:00, 23:00
13	5/11 0:00–23:00	13	5/18 0:00–8:00
14	5/12 1:00–23:00		
15	5/13 0:00–23:00		
16	5/14 0:00, 2:00–23:00		
17	5/15 1:00–2:00, 6:00–9:00		
18	5/18 17:00–18:00		

Table S2. Comparing HONO and NO_2 concentrations, as well as the HONO/NO_2 ratio at Mt. Lao with those observed at other sites.

Type	Site location	Periods	HONO (pptv)	NO_2 (ppbv)	HONO/NO_2	References
Coastal/ Islands	Mt. Lao	27 Apr–19 May 2021	456 ± 373	5.89 ± 4.80	0.13	This study
	Qingdao ("sea case")	1 Jul–25 Aug 2019	216 ± 207	3.1 ± 2.6	0.088	Yang et al. (2021)
	Coastal Shanghai	3–16 Jun 2017	650	11.05	0.059	Cui et al. (2019)
	Hok Tsui	1 Sep–19 Dec 2012	126 ± 95	4.06 ± 3.29	0.03	Zha et al. (2014)
	Cyprus	7 Jul–3 Aug 2014	35 ± 25	0.14 ± 0.12	0.33	Meusel et al. (2016)
	Changdao, Bohai	5 Oct–21 Nov 2016	270 ± 230	4.8 ± 3.3	0.057	Wen et al. (2019)
Marine	Cape Verde, North Atlantic	25 Nov–3 Dec 2015	0.84 ± 1.00	0.038 ± 0.025	0.025	Crilley et al. (2021)
	Bermuda Is, North Atlantic	17 Apr–13 May 2019	9.8 ± 12.0	0.6 ± 0.2	0.02	Zhu et al. (2022)
	Barrow, Alaska	13 Mar–14 Apr 2009	4.6 ± 3.5[d]	0.038 ± 0.021[d]	0.12[d]	Villena et al. (2011)
Urban	Beijing	1 Apr–14 May 2016	1050 ± 950	25.97 ± 15.80	0.04	Wang et al. (2017)
	Jinan	Mar–May 2016*	1040	25.8	0.052	Li et al. (2018)
	Guangzhou	27 Sep–9 Nov 2018	740 ± 700	50.8 ± 17.2	0.023	Yu et al. (2022)
	Zhengzhou	9–31 Jan 2019	2500 ± 1900	33 ± 14	0.076	Hao et al. (2020)
Rural	Dongying	8 Feb–24 Mar 2017	260 ± 280	10.41 ± 9.11	0.025	Gu et al. (2020)
	Wangdu	8 Jun–5 Jul 2014	910 ± 480	14.5	0.06	Liu et al. (2019)
	New York	26 Jun–14 Jul 1998	63 ± 33	1.1 ± 0.63[b]	0.07[c]	Zhou et al. (2002)

[a] Only the daytime data; [b] NO_x; [c] HONO/NO_x; [d] clean days.

Table S3. Summary of statistics (mean ± SD) of HONO and related parameters in the “sea case” and the “land case”.

Parameters	Sea case		Land case	
	Daytime	Nighttime	Daytime	Nighttime
HONO (ppbv)	0.42 ± 0.25	0.32 ± 0.27	0.51 ± 0.22	0.31 ± 0.20
$HONO/NO_2$	0.10 ± 0.08	0.12 ± 0.11	0.08 ± 0.05	0.06 ± 0.02
NO (ppbv)	1.3 ± 0.7	0.2 ± 0.2	1.8 ± 1.1	0.2 ± 0.1
NO_2 (ppbv)	5.1 ± 1.9	3.5 ± 2.2	8.4 ± 4.3	5.0 ± 2.3
O_3 (ppbv)	59.4 ± 10.3	59.7 ± 11.5	63.4 ± 13.3	59.9 ± 11.9
CO (ppbv)	251 ± 59	234 ± 74	335 ± 115	263 ± 87
SO_2 (ppbv)	0.7 ± 0.4	0.6 ± 0.4	1.4 ± 0.8	0.8 ± 0.3
$PM_{2.5}$ (μg m^{-3})	13.2 ± 5.8	14.9 ± 13.9	29.9 ± 22.8	21.1 ± 14.9
PM_{10} (μg m^{-3})	32.7 ± 20.1	57.3 ± 79.6	88.2 ± 95.2	135.7 ± 147.4
Sa (m^2 m^{-3})	4.71×10^{-4} $\pm 3.39\times10^{-4}$	4.57×10^{-4} $\pm 4.58\times10^{-4}$	6.51×10^{-4} $\pm 3.07\times10^{-4}$	7.54×10^{-4} $\pm 5.23\times10^{-4}$
pNO_3^- (μg m^{-3})	1.3 ± 0.5	1.4 ± 1.6	10.0 ± 3.3	2.6 ± 0.01
TEMP (°C)	15.2 ± 3.0	13.9 ± 2.2	18.7 ± 3.8	15.1 ± 3.6
RH (%)	76.3 ± 25.9	75.2 ± 24.6	47.3 ± 20.3	49.5 ± 17.9
WS (m s^{-1})	1.1 ± 0.6	1.0 ± 0.7	0.8 ± 0.5	0.5 ± 0.3
JNO_2 (s^{-1})	$4.3\times10^{-3} \pm 1.8\times10^{-3}$	–	$4.5\times10^{-3} \pm 1.8\times10^{-3}$	–

Daytime period: 07:00-17:00; Nighttime period: 17:00-07:00.

Table S4. Parameterizations used for sensitivity simulations.

HONO production pathways	Parameters	Parameter values		
		Lower	Recommended	Upper
Direct emission	$k_{emission}$	0.4%	0.8%	1.6%
$NO_2 + H_2O \xrightarrow{\text{aerosol surface}} HONO + HNO_3$	γ_a	1.6×10^{-6}	8×10^{-6}	1.6×10^{-5}
$NO_2 + H_2O \xrightarrow{\text{ground surface}} HONO + HNO_3$	γ_g	2×10^{-7}	1×10^{-6}	2×10^{-6}
$NO_2 + hv \xrightarrow{\text{aerosol surface}} HONO$	$\gamma_{a, hv}$	8×10^{-6}	4×10^{-5}	8×10^{-5}
$NO_2 + hv \xrightarrow{\text{ground surface}} HONO$	$\gamma_{g, hv}$	4×10^{-6}	2×10^{-5}	4×10^{-5}
$pNO_3^- + hv \rightarrow HONO$	$J(pNO_3^-)$	1.7×10^{-5}	8.3×10^{-5}	1.6×10^{-4}

Table S5. The relative contributions of different sources in the sensitivity tests of dust period (photochemical pollution period).

Cases	NO + OH	Direct emission	NO_2 + aerosol	NO_2 + ground	NO_2 + aerosol + $h\nu$	NO_2 + ground + $h\nu$	pNO_3^- + $h\nu$
$k_{emission}$ = 0.4%	25%(27%)	0%(1%)	5%(4%)	0%(0%)	53%(27%)	5%(7%)	12%(34%)
$k_{emission}$ = 1.6%	25%(26%)	2%(3%)`	4%(4%)	0%(0%)	52%(26%)	5%(7%)	12%(33%)
$\gamma_a = 1.6\times10^{-6}$	25%(20%)	1%(2%)	1%(1%)	0%(0%)	55%(30%)	5%(8%)	13%(39%)
$\gamma_a = 1.6\times10^{-5}$	24%(19%)	1%(1%)	9%(8%)	0%(0%)	50%(28%)	4%(7%)	12%(36%)
$\gamma_g = 1.6\times10^{-6}$	25%(20%)	1%(2%)	5%(4%)	0%(0%)	53%(29%)	5%(8%)	12%(37%)
$\gamma_g = 1.6\times10^{-5}$	25%(20%)	1%(2%)	5%(4%)	0%(1%)	53%(29%)	5%(8%)	12%(37%)
$\gamma_{a,\,h\nu} = 8\times10^{-6}$	36%(24%)	1%(2%)	9%(6%)	0%(0%)	21%(8%)	9%(10%)	24%(50%)
$\gamma_{a,\,h\nu} = 8\times10^{-5}$	20%(16%)	0%(1%)	3%(3%)	0%(0%)	66%(44%)	3%(6%)	8%(28%)
$\gamma_{g,\,h\nu} = 8\times10^{-6}$	25%(21%)	1%(2%)	5%(5%)	0%(0%)	55%(31%)	1%(2%)	13%(40%)
$\gamma_{g,\,h\nu} = 8\times10^{-5}$	24%(19%)	1%(1%)	4%(4%)	0%(0%)	50%(27%)	9%(14%)	12%(34%)
$J(pNO_3^-) = 1.7\times10^{-5}$	27%(26%)	1%(2%)	5%(6%)	0%(0%)	59%(42%)	5%(11%)	12%(12%)
$J(pNO_3^-) = 1.6\times10^{-4}$	23%(16%)	1%(1%)	4%(3%)	0%(0%)	47%(22%)	4%(6%)	20%(52%)

Figures

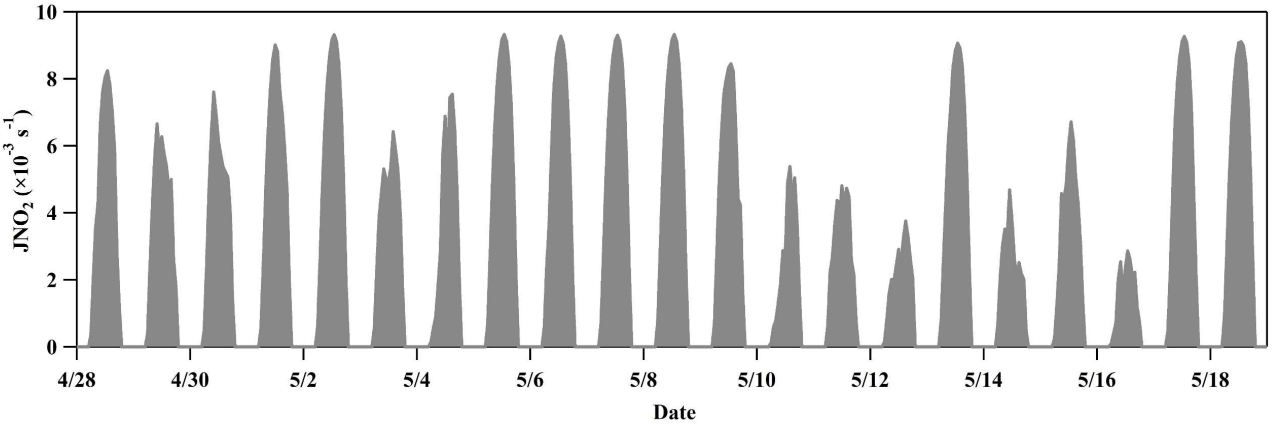

Figure S1. Time series of JNO_2 used in the model.

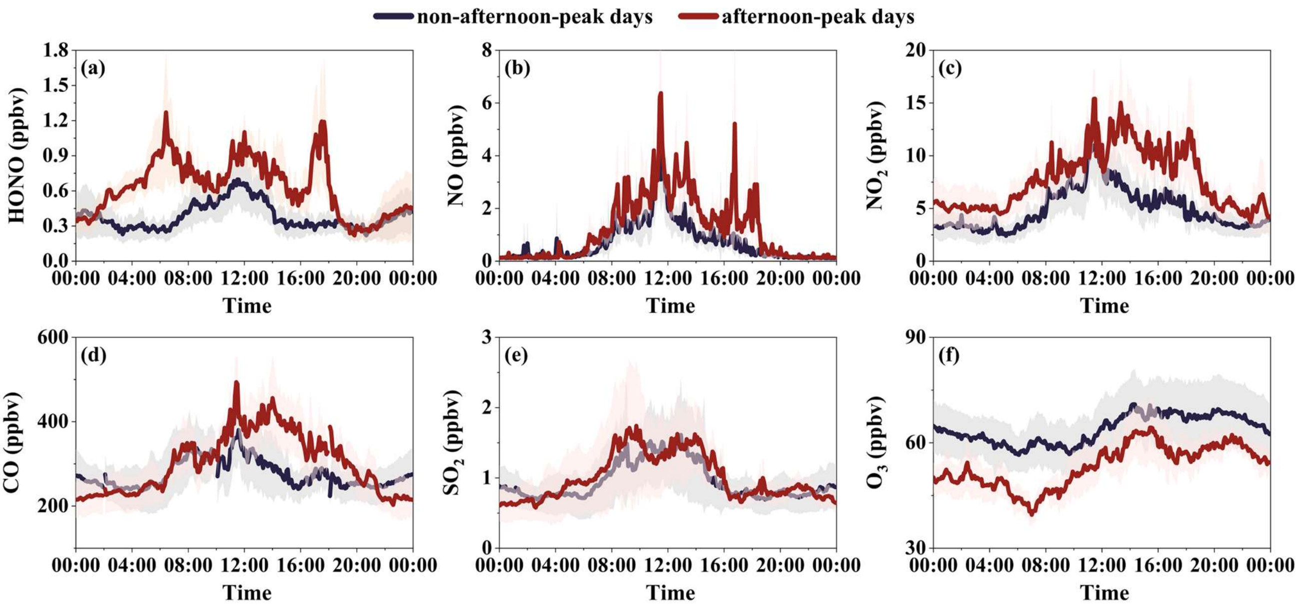

Figure S2. Comparison of diurnal variations of observed parameters in selected days with the afternoon peaks (April 27, 28, May 1, 2, 4, and 8) and overall days excluding the selected afternoon peak days.

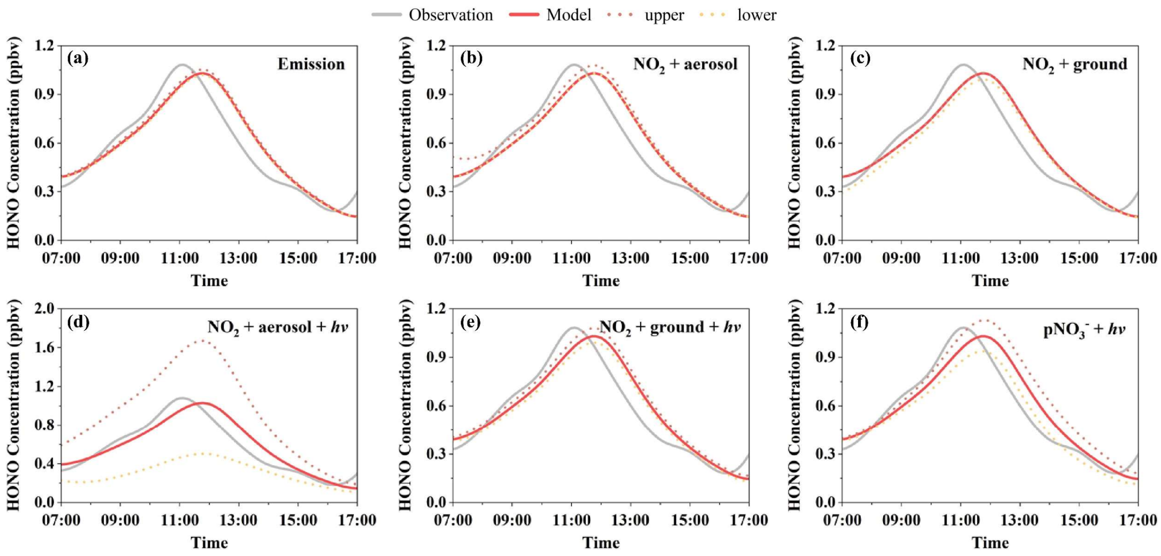

Figure S3. Sensitivity modeling results for various HONO sources during dust periods, considering both upper and lower parameter values.

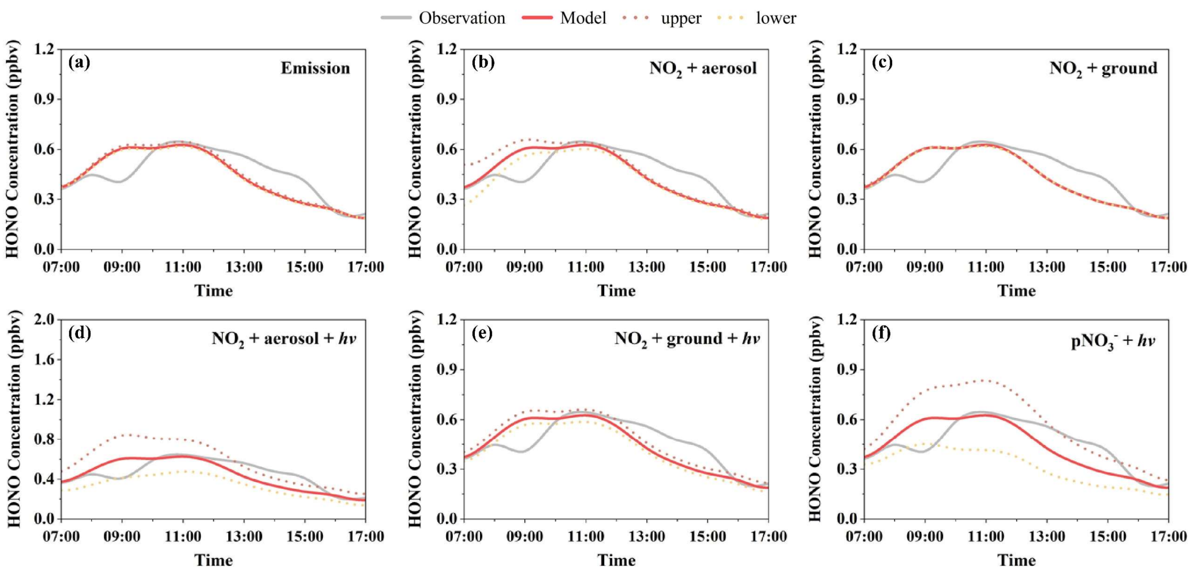

Figure S4. Sensitivity modeling results for various HONO sources during photochemical pollution periods, considering both upper and lower parameter values.

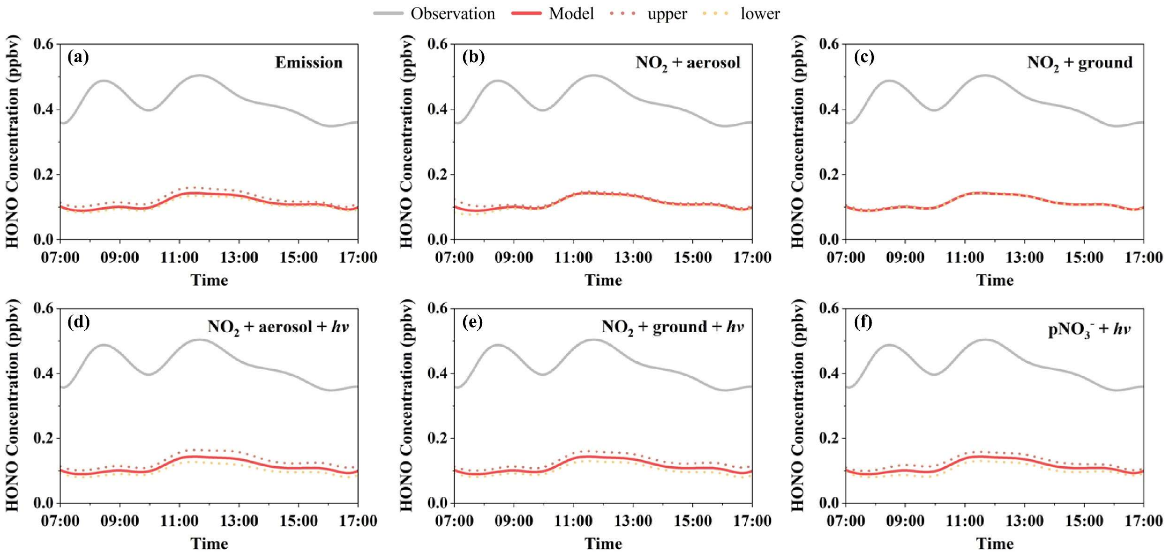

Figure S5. Sensitivity modeling results for various HONO sources in "sea case", considering both upper and lower parameter values.

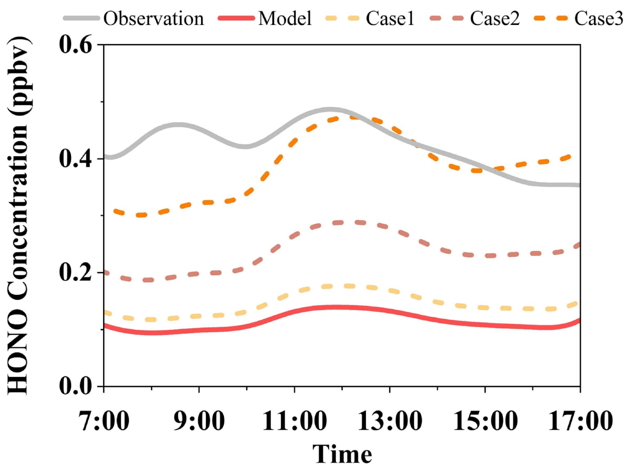

60 **Figure S6.** Model results of the sensitivity tests for NO_2 heterogeneous reactions on aerosol and ground surfaces in the "sea case". In case 1, uptake coefficients of 8×10^{-5} and 4×10^{-5} are used for aerosol and ground surfaces, respectively; in case 2, 2×10^{-4} and 1×10^{-4} are used, and in case 3, 4×10^{-4} and 2×10^{-4} are used.

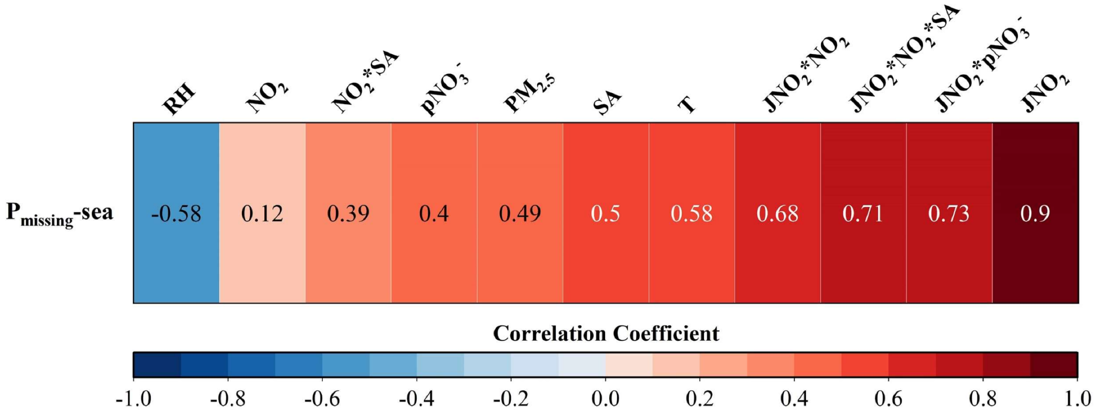

Figure S7. Correlation analysis of the daytime (7:00–17:00) missing HONO production rate ($P_{missing}$) with measured parameters in the "sea case".

References

Andersen, S. T., Carpenter, L. J., Reed, C., Lee, J. D., Chance, R., Sherwen, T., Vaughan, A. R., Stewart, J., Edwards, P. M., and Bloss, W. J.: Extensive field evidence for the release of HONO from the photolysis of nitrate aerosols, Sci. Adv., 9, eadd6266, 2023.

Crilley, L. R., Kramer, L. J., Pope, F. D., Reed, C., Lee, J. D., Carpenter, L. J., Hollis, L. D. J., Ball, S. M., and Bloss, W. J.: Is the ocean surface a source of nitrous acid (HONO) in the marine boundary layer?, Atmos. Chem. Phys., 21, 18213-18225, 10.5194/acp-21-18213-2021, 2021.

Cui, L., Li, R., Fu, H., Li, Q., Zhang, L., George, C., and Chen, J.: Formation features of nitrous acid in the offshore area of the East China Sea, Sci. Total Environ., 682, 138-150, 10.1016/j.scitotenv.2019.05.004, 2019.

Gu, R., Zheng, P., Chen, T., Dong, C., Wang, Y. n., Liu, Y., Liu, Y., Luo, Y., Han, G., Wang, X., Zhou, X., Wang, T., Wang, W., and Xue, L.: Atmospheric nitrous acid (HONO) at a rural coastal site in North China: Seasonal variations and effects of biomass burning, Atmos. Environ., 229, 117429, 10.1016/j.atmosenv.2020.117429, 2020.

Hao, Q., Jiang, N., Zhang, R., Yang, L., and Li, S.: Characteristics, sources, and reactions of nitrous acid during winter at an urban site in the Central Plains Economic Region in China, Atmos. Chem. Phys., 20, 7087-7102, 10.5194/acp-20-7087-2020, 2020.

Li, D., Xue, L., Wen, L., Wang, X., Chen, T., Mellouki, A., Chen, J., and Wang, W.: Characteristics and sources of nitrous acid in an urban atmosphere of northern China: Results from 1-yr continuous observations, Atmos. Environ., 182, 296-306, 10.1016/j.atmosenv.2018.03.033, 2018.

Liu, Y. H., Lu, K. D., Li, X., Dong, H. B., Tan, Z. F., Wang, H. C., Zou, Q., Wu, Y. S., Zeng, L. M., Hu, M., Min, K. E., Kecorius, S., Wiedensohler, A., and Zhang, Y. H.: A Comprehensive Model Test of the HONO Sources Constrained to Field Measurements at Rural North China Plain, Environ. Sci. Technol., 53, 3517-3525, 10.1021/acs.est.8b06367, 2019.

Meusel, H., Kuhn, U., Reiffs, A., Mallik, C., Harder, H., Martinez, M., Schuladen, J., Bohn, B., Parchatka, U., Crowley, J. N., Fischer, H., Tomsche, L., Novelli, A., Hoffmann, T., Janssen, R. H. H., Hartogensis, O., Pikridas, M., Vrekoussis, M., Bourtsoukidis, E., Weber, B., Lelieveld, J., Williams, J., Pöschl, U., Cheng, Y., and Su, H.: Daytime formation of nitrous acid at a coastal remote site in Cyprus indicating a common ground source of atmospheric HONO and NO, Atmos. Chem. Phys., 16, 14475-14493, 10.5194/acp-16-14475-2016, 2016.

Villena, G., Wiesen, P., Cantrell, C. A., Flocke, F., Fried, A., Hall, S. R., Hornbrook, R. S., Knapp, D., Kosciuch, E., Mauldin, R. L., McGrath, J. A., Montzka, D., Richter, D., Ullmann, K., Walega, J., Weibring, P., Weinheimer, A., Staebler, R. M., Liao, J., Huey, L. G., and Kleffmann, J.: Nitrous acid (HONO) during polar spring in Barrow, Alaska: A net source of OH radicals?, J. Geophys. Res., 116, D00R07, 10.1029/2011jd016643, 2011.

Wang, J., Zhang, X., Guo, J., Wang, Z., and Zhang, M.: Observation of nitrous acid (HONO) in Beijing, China: Seasonal variation, nocturnal formation and daytime budget, Sci. Total Environ., 587-588, 350-359, 10.1016/j.scitotenv.2017.02.159, 2017.

Wen, L., Chen, T., Zheng, P., Wu, L., Wang, X., Mellouki, A., Xue, L., and Wang, W.: Nitrous acid in marine boundary layer over eastern Bohai Sea, China: Characteristics, sources, and implications, Sci. Total Environ., 670, 282-291, 10.1016/j.scitotenv.2019.03.225, 2019.

Yang, J., Shen, H., Guo, M.-Z., Zhao, M., Jiang, Y., Chen, T., Liu, Y., Li, H., Zhu, Y., Meng, H., Wang, W., and Xue, L.: Strong marine-derived nitrous acid (HONO) production observed in the coastal atmosphere of northern China, Atmos. Environ., 244, 10.1016/j.atmosenv.2020.117948, 2021.

Yu, Y., Cheng, P., Li, H., Yang, W., Han, B., Song, W., Hu, W., Wang, X., Yuan, B., Shao, M., Huang, Z., Li, Z., Zheng, J., Wang, H., and Yu, X.: Budget of nitrous acid (HONO) at an urban site in the fall season of Guangzhou, China, Atmos. Chem. Phys., 22, 8951-8971, 10.5194/acp-22-8951-2022, 2022.

Zha, Q., Xue, L., Wang, T., Xu, Z., Yeung, C., Louie, P. K. K., and Luk, C. W. Y.: Large conversion rates of NO_2 to HNO_2 observed in air masses from the South China Sea: Evidence of strong production at sea surface?, Geophys. Res. Lett., 41, 7710-7715, 10.1002/2014gl061429, 2014.

Zhou, X., Civerolo, K., Dai, H., Huang, G., Schwab, J., and Demerjian, K.: Summertime nitrous acid chemistry in the atmospheric boundary layer at a rural site in New York State, J. Geophys. Res. Atmos., 107, ACH 13-11-ACH 13-11, 10.1029/2001jd001539, 2002.

Zhu, Y., Wang, Y., Zhou, X., Elshorbany, Y. F., Ye, C., Hayden, M., and Peters, A. J.: An investigation into the chemistry of HONO in the marine boundary layer at Tudor Hill Marine Atmospheric Observatory in Bermuda, Atmos. Chem. Phys., 22, 6327-6346, 10.5194/acp-22-6327-2022, 2022.